Ka-Band Orthogonal Load-Modulated Balanced Amplifier in 22 nm CMOS FDSOI

Jere Rusanen, Alok Sethi, Nuutti Tervo, Timo Rahkonen, Aarno Pärssinen, Veeti Kiuru, Janne P. Aikio
Department of Information Technology and Electrical Engineering, University of Oulu, Finland

***Abstract* — An integrated orthogonal load-modulated balanced amplifier (OLMBA) is designed and fabricated using 22 nm CMOS FDSOI. The input control signal in OLMBA is reflected back to balanced power amplifier (PA) pair via reactively terminated quadrature hybrid at the output in order to achieve load modulation. The proposed PA operates at third generation partnership project/new radio (3GPP/NR) 26/28 GHz Frequency Range 2 (FR2), achieving 19.5 dBm output power, 16.6 dB gain, 15.7% power added efficiency (PAE) and 18.3 dBm output 1-dB compression point (P_{1dB}), measured at 26 GHz. The PA shows excellent linearity performance with modulated signals. Using -28 dBc adjacent channel leakage ratio (ACLR) and -21.9 dB (8%) error vector magnitude as threshold values, the proposed PA achieves 11.4 dBm and 4.9 dBm average output power (P_{avg}) with 100 MHz and 400 MHz 64-QAM 3GPP/NR FR2 signal, and 14 dBm P_{avg} with 0.6 Gb/s (120 MHz) single carrier (SC) 64-QAM signal, measured at 26 GHz.**

***Keywords* — power amplifier, stacked power amplifier, fully depleted silicon-on-insulator (FDSOI), fifth generation (5G), millimeter-wave (mmWave), active matching.**

I. Introduction

Fifth generation (5G) high-throughput communications are taking place in the millimeter-wave (mmWave) frequency range, while sixth generation (6G) is envisioned to push the frequency even further [1], [2], [3]. The link range on these high frequencies is often extended with phased arrays, which require small form factor front-end circuitry due to the physically tight antenna spacing. When the number of active antenna terminals increase, the less power a single PA needs to contribute to the effective isotropic radiated power (EIRP) and therefore compact, silicon-based PAs become a feasible option [4], [5]. In contrast to the lower frequency PAs, integrated 5G mmWave PAs cannot be easily linearized with digital pre-distorter due to the wide modulation bandwidths and large number of parallel PAs to be linearized [6]. As a result, research has been ongoing for years to seek out suitable PA-solutions for mmWave 5G [7] - [15].

A relatively new technique for active load tuning, called load-modulated balanced amplifier (LMBA), has emerged beside Doherty load modulation and integrated mmWave implementations already exist [16], [17], [18]. The LMBA has further evolved into another quadrature coupler based load modulation technique, i.e. the orthogonal load-modulated balanced amplifier [19]. In OLMBA, a control signal is injected in the isolation terminal of the input quadrature coupler and the output quadrature coupler isolation port is terminated with a reactive load. The control signal is reflected back to balanced PA pair outputs, resulting in load modulation. The load seen by the balanced amplifier pair therefore depends on the control signal phase and amplitude, as well as from the choice of the reactive load.

The OLMBA is appealing in the sense that the control signal can be weak, since it is amplified by the balanced amplifier pair. As a downside, the control signal power does not directly contribute to the output power as in LMBA. Additionally, OLMBA is prone to asymmetric load modulation. This paper presents, to the author's best knowledge, the first fully integrated mmWave OLMBA, designed and fabricated using GLOBALFOUNDRIES 22 nm FDSOI [20]. The following sections provide design overview of a fixed phase prototype OLMBA, followed by extensive measurements featuring high dynamic range 5G signals.

II. Design Overview

The integrated OLMBA implementation (Fig. 1) comprises of four PA blocks and three transformer-based 50 Ω quadrature hybrids. The PA blocks are three-stacked pseudo-differential structures matched to 50 Ω. The benefit in 50 Ω matched block approach is simplicity, since all the building blocks in the line-up can be designed and treated as separate entities. Disadvantage to this approach is the increased amount of intermediate matching, along with the losses and area cost involved. Schematic of a PA block is shown in Fig. 1 (a). The main signal driver (DR) and the PA pair forming the output stage (BA1 and BA2) have total transistor width of 300 µm each, divided into two 150 µm branches, while the control amplifier (CA) has half of the width (total 150 µm). The control amplifier has a source degeneration transistor allowing better adjustment of its output power. The output quadrature hybrid has its isolation port terminated with a large capacitor, which is essentially a short circuit at the operating frequency. This choice simplifies the analysis and makes the output voltage mainly a function of the BA1 current profile. This way the input control signal essentially translates into an adjustable phase offset at the output, opening possibilities in the pursuit of linearity.

As established in [19], the balanced amplifier pair output currents depend on voltage scaling factor α, which represents the ratio of the control signal to the main input signal. The load impedances seen by BA1 and BA2 can be written as in Fig 1 (b). DR and CA are fixed at quadrature phase offset due to the coupler at the input, apart from some inevitable level of phase distortion, and so α has complex value dependent on the CA output level. Fig. 2 shows the simulated results of the load modulation, where BA1 and BA2 are at the same bias. When CA is turned on, the whole impedance trajectory is pulled

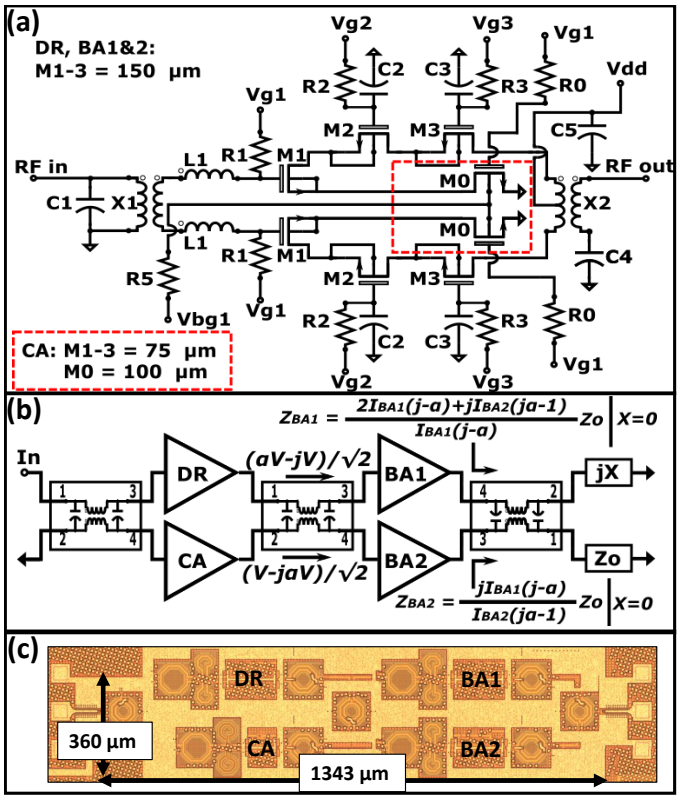

Fig. 1. a) Schematic of the PA block (CA specific parts highlighted), b) block diagram of the integrated OLMBA and c) micrograph of the fabricated PA.

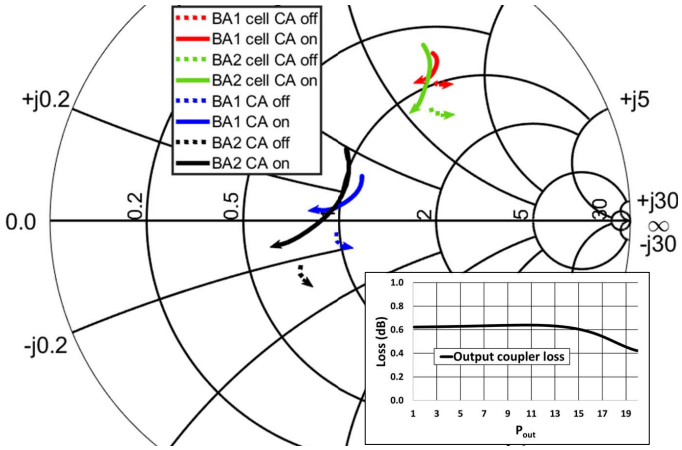

Fig. 2. Simulated load modulation and output coupler loss vs. output power. Arrow direction indicates increasing output power.

lower and as the control signal strengthens with increasing power level, the impedance is reduced further.

III. Measurement Results

A. Continuous Wave Measurements

Continuous wave (CW) power sweeps were conducted using Keysight PNA-X network analyzer and Cascade Infinity I40 probes. Input power was calibrated to the end of the input cable and the remaining 0.5 dB loss from the probe was taken into account when analyzing the results. The calibration was

Table 1. Measurement results using CW and modulated signals.

Frequency (GHz)	24	26	27	29
I_{dQ} (mA)	63.3	55.1	54.7	89
Gain (dB)	15.9	16.6	15.4	15.9
P_{sat} (dBm)	19.6	19.5	19.2	18.7
PAE/DE_{max} (%)	15.8/21.6	15.7/24.8	13.9/19	11.4/16.6
P_{1dB} (dBm)	19.3	18.3	18.3	17.8
PAE/DE at 6 dB BO from P_{1dB} (%)	7/9.4	6.8/10.9	6.7/9.2	4.4/6.6
AM-PM at P_{1dB} (°)	3.8	2.2	2.3	7.2
100 MHz 64-QAM 3GPP/NR FR2				
P_{avg} (dBm)	12.1	11.4	11.2	11.5
EVM (dB)	-23.8 (6.4 %)	-24.0 (6.3 %)	-24.3 (6.1 %)	-22.9 (7.2 %)
ACLR (dBc)	-28.1	-28.9	-28	-28.1
PAE/DE_{avg} (%)	5.7/7.8	5.6/9.3	5.6/7.7	4.3/6.7

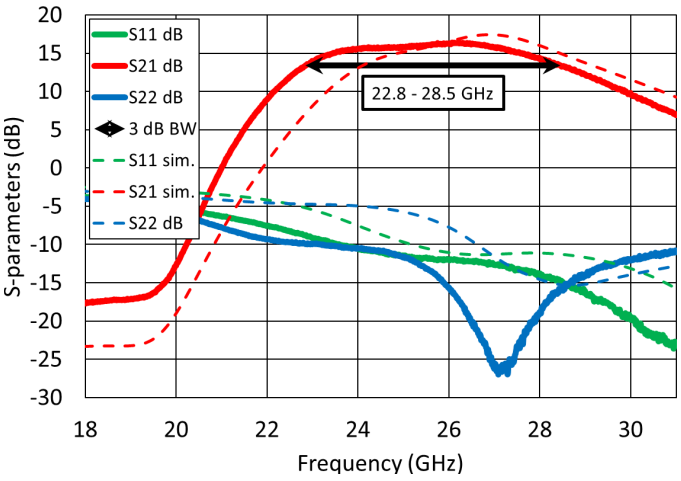

Fig. 3. Measured and simulated S-parameters (bias the same as with 26 GHz results in Table I).

normalized using external calibration substrate (Cascade P/N 101-190) and therefore the probe pads are included in the measurements.

Measured and simulated S-parameters are presented in Fig. 3 showing relatively good match. The simulations predict slightly higher frequencies predominantly because the dummy metal fills were not included in the EM models. The results show 16.5 dB gain at center frequency 26 GHz with 3-dB bandwidth spanning from 22.8 to 28.5 GHz. S11 and S22 both remain below -10 dB throughout the operating range. S12 stays below -45 dB and is omitted for clarity.

Bias voltages for the lowest gates (V_{g1}) were generated with on-chip programmable variable current sources and swept within moderate class AB for each measured frequency. Upper gate biases (V_{g2} and V_{g3}) were fixed and set with separate off-chip voltage supplies so that none of the transistors would exceed the maximum V_{ds} of 900 mV. With focus on the linearity demands of a 5G waveform, the emphasis was on achieving high output 1-dB compression point (P_{1dB}) with minimal amplitude to phase modulation (AM-PM) [23], [24]. Measurement results at different frequencies with their respective bias settings (total drain current I_{dQ}) are listed in Table 1. Fig. 4 shows an example how the load can

Table 2. Comparison to the State-of-the-Art.

	This work			**[21]**		**[17]**	**[18]**	**[22]**
Technology	22 nm FDSOI			22 nm FDSOI		65 nm CMOS	28 nm CMOS	45 nm RFSOI
Architecture	OLMBA			Doherty		LMBA	LMBA	Doherty
Frequency (GHz)	26			28		33	36	32.5
Supply (V)	2.7			2.4		1.1	1	2 & 1
Gain (dB)	16.6			26.1		10	18	-
P_{sat} (dBm)	19.5			22.5		20	22.6	22
PAE_{max} (%)	15.7			28.5		23.3	32	40.5
P_{1dB} (dBm)	18.3			21.1		-	19.6	21.5
Modulation scheme	OFDM 64-QAM		SC 64-QAM	SC 64-QAM		SC 64-QAM	SC 64-QAM	OFDM 64-QAM
Bandwidth (MHz)	100	4x100	120	-	-	-	-	200
Data rate (Gb/s	0.492	1.97	0.6	2.4	0.6	6	12	-
P_{avg} (dBm)	11.4	4.9	14	10.9	11.8	10.6	16	9.5
EVM (dB)	-24	-24.7	-26.6	-25.1	-25.1	-27	-25	-25.4
ACLR (dBc)	-28.9	-28	-28.8	-28	-28.2	-29	-	-25.8
PAE_{avg} / DE_{avg} (%)	5.6 / 9.3	1.7 / 3.1	8.8 / 13.7	9.2 / -	11.6 / -	- / 12.1	22 / -	15.5 / -
$\frac{PAE_{avg}}{PAE_{max}}$	0.36	0.11	0.56	0.32	0.41	0.32 (DE)	0.69	0.38
Area (mm^2)	0.484			0.2		1.47	1.44	0.62

be optimized both for output stage (BA1 and BA2) drain efficiency (DE) and linearity. CA pushes the impedance down, giving a penalty in gain, but resulting in better efficiency, gain flatness and phase distortion. At 6 dB back-off from P_{1dB}, the efficiency is as good as with normalized class B and 2.3 times better than class A, while all the PA blocks are operating in class AB.

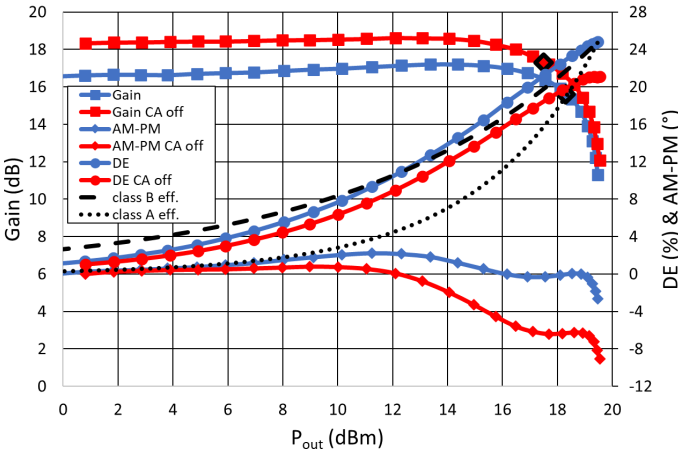

Fig. 4. CW power sweep results measured at 26 GHz.

B. *Modulated Measurements*

Modulated measurements were conducted with 100 and 400 MHz 64-QAM 3GPP/NR FR2 waveforms (10.9 dB peak to average power ratio with 1e-3 peak probability), and a 0.6 Gb/s (120 MHz) single carrier (SC) 64-QAM signal (0.35 roll-off factor). The waveforms were generated with Keysight M8190A arbitrary waveform generator and fed to Keysight E8257D programmable signal generator. The PA output was measured with Keysight N9040B UXA. Error vector magnitude (EVM) was analyzed with vector signal analyzer software (Keysight 89600 VSA). Measurement setup baseline EVM and ACLR were measured via on-chip thru to be 2.3% (-32.8 dB) and -42 dBc, respectively.

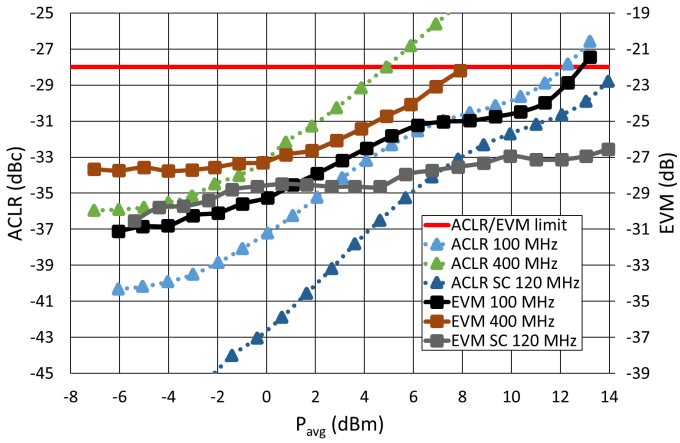

Fig. 5. ACLR and EVM measurement results at 26 GHz.

ACLR and EVM values of -28 dB and 8% (-21.9 dB) were used as threshold values for reporting the average output power, as given in 3GPP/NR base station specification [1]. The measurement results at 26 GHz are shown in Fig. 5. Lower side ACLR was observed to be the more limiting sideband on every tested frequency and therefore higher side ACLR is not shown. Measured at 26 GHz center frequency with 100 and 400 MHz 64-QAM OFDM signals, the PA reaches 11.4 dBm and 4.9 dBm P_{avg}, respectively. Worth noting with the 400 MHz signal is that the EVM limit was met with 3 dB more power, at 8 dBm P_{avg}. Results with 100 MHz signal are also summarized in Table 1, where the PA shows steady performance throughout the tested frequencies. With SC 64-QAM the PA achieves 14 dBm P_{avg} with good linearity.

C. *Comparison to the State-of-the-Art*

Measurement results at 26 GHz are compared to other state-of-the-art advanced PA solutions in Table 2. With CW results the proposed PA delivers comparable output power, gain and output compression point. With modulated signals the proposed PA compares extremely well among the the load

modulation architectures and succeeds in retaining a good backed-off to maximum PAE ratio, especially considering that SC 64-QAM can have 4-5 dB lower PAPR compared to the OFDM 64-QAM used in this work [5], [22].

IV. Conclusion

This paper reported a fully integrated OLMBA, fabricated with GLOBALFOUNDRIES 22 nm CMOS FDSOI and operating on 3GPP/NR FR2 frequency range 24.25-29.5 GHz. Measured at 26 GHz, the PA achieves P_{sat}, gain, PAE and P_{1dB} of 19.5 dBm, 16.6 dB, 15.6% and 18.3 dBm, respectively. With high dynamic range 100 and 400 MHz 64-QAM 3GPP/NR OFDM signals the PA outputs 11.4 and 4.9 dBm P_{avg} within the specifications, respectively. With 0.6 Gb/s SC 64-QAM the PA reaches 14 dBm P_{avg}. Compared to other load modulated Ka-band PAs, the prototype delivers similar or better performance with a new architecture, showing that it is a promising candidate for 5G mmWave use.

Acknowledgment

This research has been financially supported by Infotech Oulu and Academy of Finland research projects MIMEPA (grant 323779) and 6G Flagship (grant 346208). GLOBALFOUNDRIES is acknowledged for silicon processing and technical support. Author Jere Rusanen would like to thank Seppo Säynäjäkangas Science Foundation and Foundation of Riitta and Jorma J. Takanen for personal grants.

References

[1] 3GPP, "Base Station (BS) radio transmission and reception," 3rd Generation Partnership Project (3GPP), Technical Specification (TS) 38.104, 06 2021, version 17.2.0. [Online]. Available: https://www.3gpp.org/ftp/Specs/archive/38_series/38.104/38104-h20.zip

[2] M. Shafi, H. Tataria, A. F. Molisch, F. Tufvesson, and G. Tunnicliffe, "Real-Time Deployment Aspects of C-Band and Millimeter-Wave 5G-NR Systems," in *IEEE Int. Conf. Commun. (ICC)*, 2020.

[3] M. Latva-aho, *Key drivers and research challenges for 6G ubiquitous wireless intelligence*. Oulun yliopisto, 2019. [Online]. Available: http://urn.fi/urn:isbn:9789526223544

[4] V. Camarchia, R. Quaglia, A. Piacibello, D. P. Nguyen, H. Wang, and A.-V. Pham, "A Review of Technologies and Design Techniques of Millimeter-Wave Power Amplifiers," *IEEE Trans. Microw. Theory Techn.*, vol. 68, no. 7, pp. 2957–2983, 2020.

[5] H. Wang, P. M. Asbeck, and C. Fager, "Millimeter-Wave Power Amplifier Integrated Circuits for High Dynamic Range Signals," *IEEE J. Microwaves*, vol. 1, no. 1, pp. 299–316, 2021.

[6] N. Tervo, B. Khan, O. Kursu, J. P. Aikio, M. Jokinen, M. E. Leinonen, M. Juntti, T. Rahkonen, and A. Pärssinen, "Digital Predistortion of Phased-Array Transmitter With Shared Feedback and Far-Field Calibration," *IEEE Trans. Microw. Theory Techn.*, vol. 69, no. 1, pp. 1000–1015, 2021.

[7] P. M. Asbeck, N. Rostomyan, M. Özen, B. Rabet, and J. A. Jayamon, "Power Amplifiers for mm-Wave 5G Applications: Technology Comparisons and CMOS-SOI Demonstration Circuits," *IEEE Trans. Microw. Theory Techn.*, vol. 67, no. 7, pp. 3099–3109, 2019.

[8] J. A. Jayamon, J. F. Buckwalter, and P. M. Asbeck, "Multigate-Cell Stacked FET Design for Millimeter-Wave CMOS Power Amplifiers," *IEEE J. Solid-State Circuits*, vol. 51, no. 9, pp. 2027–2039, 2016.

[9] B. Park, S. Jin, D. Jeong, J. Kim, Y. Cho, K. Moon, and B. Kim, "Highly Linear mm-Wave CMOS Power Amplifier," *IEEE Trans. Microw. Theory Techn.*, vol. 64, no. 12, pp. 4535–4544, 2016.

[10] B. Kim, K. Moon, D. Jeong, S. Kim, and J. Shin, "Linear PA at mm-Wave band for 5G application," in *10th Global Symp. on Millimeter-Waves*, 2017, pp. 80–82.

[11] S. Shakib, H.-C. Park, J. Dunworth, V. Aparin, and K. Entesari, "20.6 A 28GHz efficient linear power amplifier for 5G phased arrays in 28nm bulk CMOS," in *IEEE Int. Solid-State Circuits Conf. (ISSCC)*, 2016, pp. 352–353.

[12] X. Fang, J. Xia, and S. Boumaiza, "A 28-GHz Beamforming Doherty Power Amplifier With Enhanced AM-PM Characteristic," *IEEE Trans. Microw. Theory Techn.*, vol. 68, no. 7, pp. 3017–3027, 2020.

[13] F. Wang and H. Wang, "24.1 A 24-to-30GHz Watt-Level Broadband Linear Doherty Power Amplifier with Multi-Primary Distributed-Active-Transformer Power-Combining Supporting 5G NR FR2 64-QAM with >19dBm Average Pout and >19% Average PAE," in *IEEE Int. Solid-State Circuits Conf. (ISSCC)*, 2020, pp. 362–364.

[14] N. Rostomyan, M. Özen, and P. Asbeck, "28 GHz Doherty Power Amplifier in CMOS SOI With 28% Back-Off PAE," *IEEE Microw. Wireless Compon. Lett.*, vol. 28, no. 5, pp. 446–448, 2018.

[15] F. Wang, T.-W. Li, S. Hu, and H. Wang, "A Super-Resolution Mixed-Signal Doherty Power Amplifier for Simultaneous Linearity and Efficiency Enhancement," *IEEE J. Solid-State Circuits*, vol. 54, no. 12, pp. 3421–3436, 2019.

[16] D. J. Shepphard, J. Powell, and S. C. Cripps, "An Efficient Broadband Reconfigurable Power Amplifier Using Active Load Modulation," *IEEE Microw. Wireless Compon. Lett.*, vol. 26, no. 6, pp. 443–445, 2016.

[17] C. R. Chappidi, T. Sharma, Z. Liu, and K. Sengupta, "Load Modulated Balanced mm-Wave CMOS PA with Integrated Linearity Enhancement for 5G applications," in *IEEE MTT-S Int. Microw. Symp.*, 2020, pp. 1101–1104.

[18] V. Qunaj and P. Reynaert, "26.2 A Doherty-Like Load-Modulated Balanced Power Amplifier Achieving 15.5dBm Average Pout and 20% Average PAE at a Data Rate of 18Gb/s in 28nm CMOS," in *IEEE Int. Solid-State Circuits Conf. (ISSCC)*, vol. 64, 2021, pp. 356–358.

[19] D. J. Collins, R. Quaglia, J. R. Powell, and S. C. Cripps, "The Orthogonal LMBA: A Novel RFPA Architecture With Broadband Reconfigurability," *IEEE Microw. Wireless Compon. Lett.*, vol. 30, no. 9, pp. 888–891, 2020.

[20] S. Ong *et al.*, "A 22nm FDSOI Technology Optimized for RF/mmWave Applications," in *2018 IEEE Radio Frequency Integrated Circuits Symposium (RFIC)*, 2018, pp. 72–75.

[21] Z. Zong, X. Tang, K. Khalaf, D. Yan, G. Mangraviti, J. Nguyen, Y. Liu, and P. Wambacq, "A 28-GHz SOI-CMOS Doherty Power Amplifier With a Compact Transformer-Based Output Combiner," *IEEE Trans. Microw. Theory Techn.*, vol. 69, no. 6, pp. 2795–2808, 2021.

[22] T.-Y. Huang, N. S. Mannem, S. Li, D. Jung, M.-Y. Huang, and H. Wang, "26.1 A 26-to-60GHz Continuous Coupler-Doherty Linear Power Amplifier for Over-An-Octave Back-Off Efficiency Enhancement," in *IEEE Int. Solid-State Circuits Conf. (ISSCC)*, vol. 64, 2021, pp. 354–356.

[23] S. Golara, S. Moloudi, and A. A. Abidi, "Processes of AM-PM Distortion in Large-Signal Single-FET Amplifiers," *IEEE Trans. Circuits Syst. I*, vol. 64, no. 2, pp. 245–260, 2017.

[24] U. Çelik and P. Reynaert, "Robust, Efficient Distributed Power Amplifier Achieving 96 Gbit/s With 10 dBm Average Output Power and 3.7% PAE in 22-nm FD-SOI," *IEEE J. Solid-State Circuits*, vol. 56, no. 2, pp. 382–391, 2021.